Highly stable phosphine modified VOx/Al2O3 catalyst in propane dehydrogenation

Yu Gu, Haijun Liu, Miaomiao Yang, Zhipeng Ma, Lianming Zhao, Wei Xing, Pingping Wu, Xinmei Liu, Svetlana Mintova, Peng Bai, et al.

Highly stable phosphine modified VO_x/Al_2O_3 catalyst in propane dehydrogenation

Yu Gu[a], Haijun Liu[b], Miaomiao Yang[a], Zhipeng Ma[a,c], Lianming Zhao[b], Wei Xing[b], Pingping Wu[a], Xinmei Liu[a], Svetlana Mintova[a,d], Peng Bai[a,*], and Zifeng Yan[a,*]

[a] State Key Laboratory of Heavy Oil Processing, College of Chemical Engineering, China University of Petroleum (East China), Qingdao, 266580, China

[b] School of Science, China University of Petroleum (East China), Qingdao, 266580, China

[c] School of Chemical Engineering, The University of New South Wales, Sydney, NSW 2052, Australia

[d] Normandie University, ENSICAEN, UNICAEN, CNRS, Laboratoire Catalyse et Spectrochimie, 14000 Caen, France

* Corresponding authors

E-mail: baipeng@upc.edu.cn (P. Bai)

zfyancat@upc.edu.cn (Z. Yan)

Abstract

The relatively low cost and mild toxicity of vanadium makes it an alternative to commercially applied Pt and Cr based catalysts in propane dehydrogenation (PDH). Conventional VO_x/Al_2O_3 catalyst shows high initial activity, but deactivates fast due to severe coke formation, which requires frequent regeneration by coke combustion and causes massive CO_2 emissions. In this context, we report on the phosphine (PH_3) surface modification of VO_x/Al_2O_3 catalyst leading to substantial improvement of its stability. The phosphorus considerably modifies the properties of the VO_x/Al_2O_3 catalyst: (i) tunes surface acidity, (ii) separates polymerized vanadium oxide species and (iii) weakens interaction between vanadium species with alumina support. Synergy among all these factors facilitate desorption of produced propylene and inhibit the oligomerization of coke precursors, which contributed to the enhancement of the catalyst stability during propane dehydrogenation.

Keywords: Phosphine modification, stability enhancement, propane dehydrogenation, coking, propylene desorption

1. Introduction

Propylene is a fundamental chemical raw material that can be used to produce a variety of downstream derivatives such as polypropylene, acrylonitrile, isopropanol, acetone and epoxypropane[1, 2]. Currently, propylene is mainly produced by steam cracking and fluid catalytic cracking processes[2, 3]. However, the foregoing two processes are high energy-consuming and could not meet the globally increasing demand for propylene due to crude oil dependence, thus are not economically and environmentally friendly. Propane dehydrogenation, as an alternative process which could produce highly value-added propylene using cheap propane from clean energy source such as shale gas and natural gas as a raw material, has attracted increasing attentions in past few decades[4]. The development of propane dehydrogenation could be one of the most efficient and clean solutions for propylene supply.

Two different processes of propane dehydrogenation have been studied in recent years, which are oxidative dehydrogenation (ODH) of propane and non-oxidative dehydrogenation of propane (PDH). ODH is a fascinating technology with high conversion and energy saving due to the oxidation of hydrogen by oxidants such as oxygen, carbon dioxide and nitric oxide[5-7]. However, the obstacle of this technology, the low selectivity towards propylene caused by over-oxidation, still could not be overcome so far[7]. PDH has been commercialized as Oleflex (Honeywell UOP) and Catofin (ABB Lummus) processes using Pt and Cr based catalysts respectively[8, 9]. Nevertheless, the high cost of platinum, toxicity of chromia and fast deactivation of both of them have posed economic and environmental issues[10, 11].

As an alternative, vanadium-based catalysts have been widely investigated since 1980s due to its high activity in oxidative dehydrogenation of lower alkanes[12]. Recently, supported VO_x catalysts were found to be active in non-oxidative dehydrogenation of lower alkanes and

successfully regenerated for several cycles[13, 14]. But, in a single dehydrogenation run, the catalyst deactivates fast due to coke deposition and requires frequent regeneration by combusting coke, which causes massive CO_2 emission. Modification of catalysts with non-metal elements, such as sulfur, is one of the solutions applied. Li et al. introduced sulfur into supported metal oxide catalysts, and the modified catalysts exhibited enhanced stability and selectivity toward olefins by deactivating the most active hydrogenolysis sites[15, 16]. However, a gradual sulfur loss occurred during the reaction and the continuous co-feeding of H_2S was needed to maintain a stable catalytic performance. Phosphorus has been used to modify industrial hydrotreating catalysts previously due to the strong interaction between phosphate and alumina. Recently, Tan et al. also reported the enhanced performance of Fe/P/Al catalyst in PDH by phosphorous doping, and phosphorus was found to induce the formation of active Fe_3C sites and significantly improved C_3H_6 selectivity[17]. Nevertheless, as phosphorus was commonly introduced as phosphoric acid or phosphate by wetness impregnation, aluminum phosphate forms with a significant reduction in surface area and blocking of pore openings[18-20]. To circumvent these Liu et al. developed an elegant approach towards preparation of Ni_2P/Al_2O_3 hydrodesulfurization catalyst using gaseous PH_3 as the phosphiding agent, which eliminated the formation of aluminum phosphate[21].

In this context, we modified VO_x/Al_2O_3 catalysts in propane dehydrogenation with PH_3 surface treatment, which leads to great improvement of catalyst stability by inhibiting coking deposition during propane dehydrogenation. Experimental results revealed that the synergy among tuned acidity, lower coking precursor intimacy and faster propylene desorption after phosphorus modification accounted for the enhancement in catalytic stability during propane dehydrogenation.

2. Experimental

2.1. Catalyst preparation

VO_x/Al_2O_3 was synthesized via incipient wetness impregnation. In a typical procedure, 6.944 g of ammonium metavanadate (Alfa Aesar, USA) was dissolved together with 19.128 g oxalic acid dehydrate (Sinopharm, China) in 60 mL deionized water at 343 K. After stirring, the solution turned into dark blue. Then 40 g pseudo boehmite (Henghui Chemical, China) was added into the dark blue solution resulted in a muddy mixture. Then the mixture was fully stirred for 10 minutes and dried at 343 K for 4 h in air, followed by additional desiccation at 373K overnight to obtain a dried precursor. Calcination of the precursor was conducted in a muffle furnace (Nabertherm, Germany) at 823 K for 10 h with a ramp rate of 2 K/min. After cooling to room temperature, the VO_x/Al_2O_3 catalyst with 10 wt% vanadium loading was prepared (PV-0).

Phosphine modification of the VO_x/Al_2O_3 catalyst was carried out in a chemical vapor deposition system (Nabertherm, Germany). Sodium hypophosphite monohydrate (Sionpharm, China) was put upstream in a crucible placed in the quartz tube, and the VO_x/Al_2O_3 was placed in the downstream. Nitrogen was used as a carrier gas and flowed into the closed system continuously. Temperature was elevated to 393 K and hold for 45 minutes to remove the moisture. Then the tube was further heated to 573 K with a ramp rate of 2 K/min and hold for 1 h. During this period, sodium hypophosphite decomposed and released PH_3 gas according to the eq. (1).

$$2NaH_2PO_2 \rightarrow Na_2HPO_4 + PH_3\uparrow \qquad (1)$$

After that, the heating was stopped and N_2 was introduced to purge the container overnight. The exhaust gas was bubbled into a flask containing excessive amount of copper sulfate (Sinopharm, China) solution, which was used as an indicator of the phosphine formation. The exhaust phosphine reacted with copper sulfate and resulted in the formation of dark precipitates. After

phosphine modification, resulting catalysts were denoted as PV-x, where x represents the molar ratio of phosphorus to vanadium (P/V) in the final catalysts.

2.2. Catalyst characterizations

Elemental composition of samples after phosphine modification was measured on a VISTA-MPX inductively coupled plasma optical emission spectrometer (ICP-OES, Varian, USA) equipped with a CCD detector.

Coking behavior of catalysts was analyzed by thermogravimetric-differential thermal analysis (TG-DTA) measured on a HCT-1 thermal differential analyzer (Beijing Hengjiu, China) under air flow. Below 320 K, the temperature ramp was set as low as 0.33 K/min to remove most of the moisture. Then the temperature was elevated to 930 K with a ramp rate of 10 K/min. The duration time for the two periods is 30 min and 60 min, respectively.

Energy dispersive X-ray (EDX) elemental mapping was recorded on a JSM-7500F scanning electron microscope (JEOL, Japan) equipped with an X-MAX^N EDS detector (Oxford Instruments, UK). The electron accelerating voltage was set as 30 kV.

Surface acidic properties of catalysts were determined by both pyridine adsorption Fourier transform diffusing reflectance infrared spectroscopy (Py-DRIFTS) and NH_3 temperature programmed desorption (NH_3-TPD). Prior to Py-DRIFTS measurements, all samples with different P/V ratios were pretreated at 573 K for 3 h to remove moisture. Then they were placed in a desiccator with an open beaker filled with pyridine for 24 h to obtain adsorption saturation balance. After that all samples were heated at 423 K under vacuum for 3 h to remove physically absorbed pyridine. Additionally, the corresponding samples without pyridine adsorption were dehydrated at 573 K for 3 h as blank references. Ammonia temperature programmed desorption (NH_3-TPD) was conducted on an AutoChem II 2920 chemisorption analyzer (Micromeritics, USA)

equipped with a thermal conductivity detector (TCD). 0.1-0.2 g of catalyst (20-40 mesh) was packed in the middle of a U-shaped quartz tube. Prior to analysis, the samples were outgassed in an Ar flow (80 mL/min) at 573 K for 2 h. After cooling down to 353 K, the samples were saturated with NH_3 under a flow of 20 vol% (Balanced with Helium, total flow:25 mL/min) for 30-40 min. Then N_2 gas was flowed over catalyst (50 mL/min) for 30 min to remove physically adsorbed NH_3. Temperature was increased from 313 K to 850 K under N_2 flow to obtain the TPD profile.

X-ray powder diffraction (XRD) patterns were measured on an X'Pert Pro MPD diffractometer (PANalytical, Netherland) using a nickel filtered Cu $K\alpha$ radiation (λ= 0.1542 nm) at 35 kV and 40 mA in the 2θ range of 5° to 75°.

Textual properties of catalysts were determined by N_2 adsorption-desorption isotherms obtained on a TriStar 3000 (Micromeritics, USA). Prior to testing, samples were degassed in vacuum at 573 K for 4 h. The specific surface areas were calculated at the relative pressure P/P_0 of 0.05-0.25 using Brunauer-Emmett-Teller (BET) equation. Pore diameters were derived from Barrett-Joyner-Halenda (BJH) equation using the adsorption branch of isotherms.

Ultraviolet-visible diffuse reflectance spectra (UV-Vis DRS) were acquired on a SPECORD 210 plus (Analytikjena, Germany) spectrometer in the range of 200-800 nm; $BaSO_4$ (Aladdin, USA) was mixed with samples with a mass ratio of 4:1.

Raman spectra of powder samples were obtained on a DXR Raman spectrophotometer (Thermo Fisher Scientific, USA). Spectra were recorded at ambient temperature with an excitation source of 532 nm.

Fourier transform transmission infrared (FTIR) spectra were recorded on a Nicolet 6700 infrared spectrometer (Thermo Fisher Scientific, USA) equipped with a Mercury Cadmium Telluride

(MCT) detector and a KBr beam splitter. Self-supporting wafers of samples were prepared with KBr.

X-ray Photoelectron Spectroscopy (XPS) data were acquired on an ESCALAB 250Xi instrument (Thermo Fisher Scientific, USA) with an 18.2 W laser monochromatic Al *Kα* radiation. Total acquisition time of 5.25 min, pass energy of 30.0 eV and energy step size of 0.10 eV were applied. The reported binding energies were referenced to C 1S at 284.8 eV. Surface atomic ratio and vanadium species valences were determined by fitting peak XPSPEAK 41 program.

2.3. Evaluation of catalysts in propane dehydrogenation

The catalysts were tested in a continuous-flow fixed-bed micro-reactor (Tianda Beiyang Chemical Equipment Co., Ltd. China) at ambient pressure. Catalysts with different P/V ratios were pelleted, crushed and sieved into 20-60 mesh. 1.0 g catalyst was packed in the middle of a stainless steel tube (length of 500 mm, diameter of 10 mm and thickness of 3 mm), with a thermocouple inside and loaded in the middle of the catalyst bed. Thereafter, the reactor was heated to 863 K within 2 h in N_2 with a flow rate of 30 mL/min. Then the gas flow was switched to H_2 with a flow rate of 30 mL/min to conduct reduction for 2 h. Before evaluation, the reaction temperature was further increased to 883 K. Then the feed gas with a total flow rate of 30 mL/min containing propane and nitrogen with a ratio of 1:4 was pumped into the reactor. Products were analyzed by an online Agilent 7820A GC equipped with a flame ionization detector (FID) and a HP-PONA capillary column.

Conversion of propane, propylene yield and propylene selectivity were calculated based on the carbon atom balance according to the equations listed below:

$$X=\frac{N_{Propane}^{Inlet}-N_{Propane}^{Outlet}}{N_{Propane}^{Inlet}}$$

$$Y=\frac{N_{Propylene}^{Outlet}}{N_{Propane}^{Inlet}}$$

$$S=Y/X,$$

X, Y, S, N represent conversion of propane, yield of propylene, selectivity to propylene and molar amounts of gases, respectively.

3. Results and discussion

3.1. Catalytic performance

Fig. 1 shows the performance of different samples in PDH reaction. The parent catalyst (PV-0) undergoes an induction period of 1.5 h, during which the conversion (initial reactivity) increases gradually to its maximum of around 73%, then decreases dramatically to only 25% at time on stream (TOS) of 8 hours, which is the lowest conversion among all tested samples. The rapid deactivation of the parent catalyst indicates a poor stability, though it has the highest initial reactivity. In contrast, after phosphine modification, the initial reactivity of the catalysts is reduced to different extents, while conversion curves become more and more flat with the increase of phosphorus amount. All phosphine modified samples have similar induction period. The difference between the samples is observed in the following 6.5 hours after induction period (1.5 h). Samples PV-0.59, PV-0.62 and PV-0.70 still retain a conversion of approximately 45% at TOS of 8 h, almost twice higher than the parent catalyst. Sample PV-0.86 exhibits the lowest initial reactivity, but with the highest stability. The propane conversion remains almost constant (about 28%). After phosphine modification, vanadium based catalyst lost part of its reactivity, while the stability was pronouncedly enhanced.

For the parent catalyst, the propylene selectivity increases and the maximum at TOS of 3.5 h is observed, and then decreased quickly due to catalysts deactivation. For the modified catalysts, selectivity is more steady than that of the parent catalyst. With increasing P/V ratio, the average propylene selectivity drops first and then rises above that measured for the parent catalyst. For phosphine modified catalysts (PV-0.59, 0.62 and 0.86), the selectivity shows interesting rising trend as a function of time. Among all samples, PV-0.86 exhibits the highest C_3H_6 selectivity at TOS of 8 h.

By-products are analyzed and their yield and selectivity are presented in Fig. S1. The by-products are mainly C1-C2 hydrocarbons, and products with more than 3 carbon atoms are excluded due to their rather small quantity (<1%). The C1+C2 products show similar trend as that of propylene, which is caused by variations of propane conversion. With respect to C1+C2 selectivity, parent catalyst demonstrates a valley-shaped curve which is opposite to its propylene selectivity. This indicates that in the early stage of reaction, the parent catalyst tends to catalyze dehydrogenation after the induction period. After the first 4 h, deactivation happens and cracking dominates, which produces a significant amount of methane and C2. This phenomenon is consistent with the decrease in propylene selectivity of parent catalyst. In contrast, phosphine modified catalysts have better performance in resisting cracking. With increasing phosphorus amount, the C1+C2 selectivity decays. Analyses of by-products again confirm that after PH_3-treatment, the catalysts stability is greatly improved.

In summary, the stability of PH_3- modified catalysts was improved at the expense of partial loss of initial reactivity. Nevertheless, with increasing the P/V ratio, the loss of initial reactivity reduced. At TOS of 8 h, parent catalyst lost 66% of its initial reactivity, while the PV-0.86 catalyst keeps almost 91% of the initial reactivity. Furthermore, reactivity of catalysts in terms of conversion

remaining percentage (Defined as conversion at TOS=8h divided by maximum conversion) has a well-fitted linear relation as a function of the P/V ratio (Fig. 2).

3.2. Coking of catalysts

Since coking has been well recognized as the main reason for catalyst deactivation[1], the coke amount is closely related to catalyst stability. TG-DTA curves of used catalysts after 8 h of reactions are present in Fig. 3, and the coke amount is summarized in Table S1. Below 320 K, the temperature ramp was set as low as 0.33 K/min to remove the moisture from the used catalysts, which is demonstrated by steep weight loss at around 300 K. For all samples, weight loss bellow 400 K is ascribed to the removal of physically absorbed water; a small endothermal peaks in DTA curves correspond to dehydration of catalysts. The sharp decline in weight starting at 700 K is due to combustion of surface carbon species, which is also confirmed by the exothermal peak in DTA curves (Fig. 3). As shown, the amount of coke deposition decreases on the phosphine modified catalysts with increasing P/V ratio. Moreover, negligible weight loss and heat release of sample PV-0.86 suggest that almost no coke remains on the catalyst surface. This is also confirmed by the grey color of this catalyst after 8 h of reaction, while other catalysts display a black color. Combining the results of carbon deposition with the performance of the catalysts in dehydrogenation reaction, it could be concluded that the carbon deposition may be the dominant factor for catalysts deactivation. The introduction of phosphorus could efficiently suppress coke formation during propane dehydrogenation process.

In addition, EDX mapping was performed to determine the distribution of surface elements. Compared to parent catalyst, the amount of carbon deposits in phosphine modified catalysts is relatively lower, especially in the used catalyst PV-0.86 (Fig. S2c). The profiles of phosphorus

highly coincide with those of aluminum and vanadium, which indicates strong intimacy between phosphorus, vanadium species and alumina support.

3.3. Acidic properties of phosphine modified catalysts

Surface acidic property is a key factor influencing the catalyst performance in PDH reaction and it is highly related to their coking behavior. To investigate variations in surface acid sites, NH_3-TPD, transmission IR and Py-DRIFTS measurements were conducted.

NH_3-TPD measurements were performed to evaluate total acid amounts of parent and phosphine modified catalysts. In general, as the amount of phosphorus increases, concentration of total acid sites decreases (Fig. S3). It has been widely accepted that VO_x/Al_2O_3 is a bifunctional catalyst while acid sites facilitate adsorption of propane and vanadium species induce formation of active intermediate[1, 22]. Decreasing acid amount weakens the adsorption of reactants on catalysts but favors the desorption of propylene, which inhibits deeper side reactions and lengthens catalyst life span, however at the expense of lowering their activity to some extent.

Py-DRIFTS characterization was conducted to understand the nature of acid sites of the catalysts. A peak centered at 1540 cm^{-1} is attributed to Brønsted acid sites, while a peak at 1450 cm^{-1} is ascribed to Lewis acid sites (Fig. 4a). Results from the quantitative analysis are presented in Table S2a. Generally, amount of Brønsted acid sites increases after PH_3 modification, which could also be confirmed by the P-OH vibration peak 1133 cm^{-1} in transmission IR spectra (Fig. S4). After phosphine modification, amount of Lewis acid sites decreases gradually and a small blue shift to higher wavenumber is indicating the strengthening of acidity. Similar variations of BAS and LAS in phosphoric acid treated alumina and zeolites were observed previously[23, 24]. The increase in Lewis acid strength is due to the increase of aluminum unsaturation degree. This is verified by the decrease in the intensity of penta-coordinated aluminum sites (Al_V) and increase in the intensity of tetra-coordinated aluminum sites (Al_{IV}). Peaks at 1653, 1638, 1595 cm^{-1} are assigned to pyridine

adsorbed on Al_{III}, Al_{IV} and Al_{V}, respectively[25, 26]. According to Dong et al., the difference in acidic strength between Al_{III} and Al_{IV} is not significant, while Al_{V} has obviously weaker acidic strength than both of Al_{III} and Al_{IV}[27]. These results indicate that phosphine tends to eliminate weaker LAS on the surface of alumina support. Previous works reported that LAS is critical for activating propane molecule and desorption of propylene[28, 29]. Rodemerck et al. found that bare alumina (possessing only LAS formed by surface coordinatively unsaturated aluminum sites) exhibited unexpected high activity in isobutane dehydrogenation, and after hydrothermal treatment, significant amount of LAS changed to BAS and catalytic products switched to heavy coke[30], indicating significant influence of LAS on activating alkane and olefin selectivity.

BAS and LAS amounts of used catalysts are calculated and presented in Fig. 4b and Table S2b. After 8 hours of reactions, parent catalyst (PV-0) lost almost all BAS and LAS, which is consistent with its lowest activity among all tested catalysts. For phosphine modified catalysts, the more the phosphorus content is, the larger the amount of LAS remains. Besides, the intensity variations of all aluminum corresponding LAS (Al_{III}, Al_{IV} and Al_{V}) has same trends as fresh catalysts, which is also indicating better remaining of LAS with increasing the phosphorus content. The highest remaining amount of LAS on catalyst PV-0.86 (61% remaining) correlates well with the best catalytic stability (almost no deactivation). It is noteworthy that the activity is not solely related to acidity. For catalysts PV-0.62 and PV-0.70 with less LAS than that of PV-0.86 still have higher activity at TOS of 8 h. Hence, the special function of LAS in propane dehydrogenation could partially explain the decrease of initial activity and the enhancement of stability of the phosphine modified catalysts by the losses of surface LAS and increased Lewis acidic strength.

3.4. Evolution of surface vanadia species

Except for surface acidity variations, the PH_3 treatment may also affect polymerization degree of surface vanadia species, which is another key factor influencing the reactivity of catalysts[8, 13, 31]. Therefore, detailed characterizations of the evolution of surface vanadia species were conducted.

XRD patterns of different catalysts contain peaks at 37°, 45.9° and 66.9° (Fig. S5), which are attributed to γ-Al_2O_3 phase (JCPDS Card No. 10-0425)[10]. Besides, no other diffraction peaks are present in the patterns, indicating the high dispersion of surface VO_x species on alumina[32]. Moreover, XRD patterns of samples modified by phosphine show no difference with that of parent sample, indicating that the modification did not change crystalline phase of the vanadium-based catalysts and/or the new phases formed by P-modification are in trace amounts.

Textural properties of all catalysts are listed in Table S3. All samples present typical type-Ⅳ isotherms with H-2 hysteresis loops (Fig. S6), implying an ink-bottle mesoporous structure[14]. All modified catalysts exhibit slightly lower (18% in average) BET specific area in comparison to parent catalyst. BJH diameter remains almost unchanged and pore volume decreases slightly, indicating that most phosphorus atoms exist on the surface of catalysts instead of accumulating in pores. N_2 physisorption data, together with the XRD analysis indicate that the introduction of PH_3 only modified the catalyst surface without significant changes of their textural and crystalline structure, which exhibits great advantages over conventional phosphorus modifications by introducing phosphoric acid or phosphate.

Surface species on the catalysts were identified by Raman spectroscopy since alumina shows very weak absorption band in the range of 1100-100 cm^{-1}[33]. Fig. 5 shows the Raman spectra of different samples. For parent catalyst, a relatively sharp band in the range of 950-1050 cm^{-1} is observed, which is ascribed to V=O stretching vibration, indicating existence of isolated and

polymerized vanadium species[34-36]. Broad Raman band in the range 500-950 cm^{-1} can be attributed to V-O-V stretching and V-O-Al antisymmetric/symmetric stretching vibrations in polymerized VO_x[22, 35]. The sharp but low intensity peak at 145 cm^{-1} represents crystalline vanadia[37]. Comparing with the parent sample, all modified samples contain similar but relatively weaker bands in the range of 500-950 cm^{-1}. Decrease in the intensity of V-O-V and V-O-Al bands confirms that the concentration of V-O-V and V-O-Al is lower than that in parent catalyst. Peak at 145 cm^{-1} of crystalline vanadia also disappears, indicating the decrease in vanadia polymerization degree. After phosphine modification of catalysts, newly formed phosphorus species replaced partially polymerized vanadia species anchored on alumina surface. This is also confirmed by the presence of a new band at 1015cm^{-1}, characteristic of V=O stretching mode in isolated tetrahedral-coordinated VO_4[14, 35, 36, 38, 39], indicating the presence of more isolated vanadium species. Besides, the strong band at 923 cm^{-1} could be ascribed to asymmetric P-O-P vibrations of $P_2O_7^{2-}$[40-42], while the rather weak band from 1140 cm^{-1} to 1180 cm^{-1} is attributed to the V-O-P stretching of $(VO)_2P_2O_7$ as suggested by Wu et.al[42], indicating the existence of very small amount of VPO species. In summary, Raman study confirms the existence of PO_x and VO_x species and ascertain that the phosphorus modification results in the formation of more isolated vanadium species by inserting phosphorus into polymerized vanadium oxides.

Further, the status of VO_x species on different catalysts were characterized by UV-Vis DRS (Fig. 6). All spectra contain broad bands centered at 275, 310 and 350 nm due to $O^{2-} \rightarrow V^{5+}$ ligand-metal charge transfer (LMCT). These are ascribed to surface isolated and low polymerized vanadium species[14, 38, 43]. The relatively weak band at 350-400 nm is attributed to tetrahedral-coordinated and distorted octahedral-coordinated vanadium species, which indicate the existence of highly polymerized vanadium species[14]. After PH_3 surface modification of the catalysts, the

bands in this range become weaker, and the band at 275 cm^{-1} becomes dominant, suggesting the decrease in concentration of highly polymerized vanadium species, which is in line with Raman results, evidencing that more isolated and oligomeric vanadia were produced due to the insertion of phosphorus. For modified samples, a new band at 208 nm emerges, which can be assigned to $O^{2-} \rightarrow V^{4+}$ LMCT[41], implying that more V^{4+} species were presented on the surface[44]. This may be caused by PH_3 reduction of V^{5+} to V^{4+}during surface reaction. Besides, no band above 500 nm is observed, which is characteristic for the d-d transitions of V^{4+} and V^{3+}, implying the absence of trivalent vanadium species on the catalysts surface[45, 46]. Thus the V^{5+} and V^{4+} vanadium species are dominating in all samples. After phosphine modification of catalysts, more reduced tetravalent vanadium, and more isolated and low-polymerized vanadium species are formed.

Band gap energy (E_g) could reflect surface coordination states of vanadium species (Table S4). E_g is calculated according to the formula: $Eg=1240/\lambda_g$, where λ_g is determined by the intersectional point of the vertical and horizontal parts of the spectra presented in Fig. 6[22]. An obvious blue shift of E_g is observed after phosphine modification of catalysts and E_g becomes even larger with the increase of the P/V ratio of the catalysts. In our previous work, we have found that the increase of surface vanadium species will decrease band gap energy, evidencing more polymerized vanadium species[34]. The blue shift of band gap energy after phosphine modification of catalysts shows a reverse trend that the polymerized vanadium species are separated, forming more isolated ones[22]. This phenomenon was also reported before for VPO[41] and other phosphorus modified catalysts[47]. The variation of band gap energy observed is consistent with the Raman results discussed above.

Combining XRD, N_2 sorption, Raman and UV-Vis results, we could conclude that during phosphine surface modification of catalysts, the phosphorous atoms interact with alumina support

and separate polymerized vanadia species thus causing decrease in their polymerization. More isolated and low oligomeric vanadia species lead to lower initial reactivity. Nevertheless, this also inhibits the condensation of coking precursors, thus improving the catalysts stability.

3.5. Correlation between electronic effects and catalytic performance of phosphine modified samples

To further explore the nature of VO_x on PH_3 modified catalysts, XPS study on samples PV-0, PV-0.70 and PV-0.86 before and after reactions was conducted. Fig. 7 demonstrates binding energies of vanadium atoms with different valences. The characteristic V $2p_{3/2}$ peak was fitted and deconvoluted into 2 peaks for fresh catalysts ascribed to pentavalent and tetravalent vanadium oxidation states[14, 35, 36]. Trivalent vanadium species were not taken into consideration since the reduction temperature of pentavalent vanadium to trivalent vanadium is usually above 773K under reduction atmosphere[48] (PH_3 surface modification of sample was conducted at 573K for 1 h). The absence of V^{3+} is also verified by aforementioned UV-Vis study. For the used catalysts (8 h), the V $2p_{3/2}$ peak was deconvoluted into 3 peaks including V^{3+}. As shown, after PDH reaction, binding energies of V^{5+} and V^{4+} are slightly higher than for the fresh catalysts due to the presence of carbonaceous deposit[49]. It can also be observed that binding energies decrease with increasing P/V ratio for both fresh and used catalysts, indicating the weakened interaction between vanadium species with alumina support caused by phosphorus modification[50]. Previously it was reported that higher electron density leads to lower binding energy[51]. The higher electron density of vanadium caused by weaker interaction with alumina support makes it more repulsive to olefin intermediates or propylene product, thus facilitating their desorption from catalyst surface and inhibiting deep side-reactions[52], resulting in the enhanced selectivity and better stability.

On the other hand, the state of vanadium cations also has significant influence on the catalytic performance of materials. After PH_3 modification, the content of surface V^{4+} on fresh catalysts

increases (Fig. 7). After dehydrogenation reactions, the content of V^{5+} drops dramatically and the V^{4+} and V^{3+} amount increases due to the reduction of pentavalent vanadium species. The amount of V^{4+} andV^{3+} species in the catalysts is directly related with the catalysts activity. It can be seen that the used PV-0.70 catalyst contains more vanadium cations with lower valence (+3 and +4) than the used PV-0 and PV-0.86 catalysts (Fig. 7); final C_3H_8 conversion for PV-0.70 catalyst is also much higher (Fig. 1). According to previous studies, both V^{3+} and V^{4+} are more active than V^{5+} in dehydrogenation reactions[8, 22, 53]. Rajan et al. found that phosphorus could stabilize trivalent vanadium in the VPO catalyst[41]. Thus the higher content of lower valence vanadium species for used PV-0.70 and its higher final conversion may provide further explanation to the stability enhancement.

In summary, XPS data provide information about the electronic effects and catalytic performance of phosphine modified samples. Phosphine modification of catalysts weakened the interaction between vanadium species and alumina support, which makes it more repulsive to olefin intermediates or propylene product, thus facilitating their desorption from catalyst surface and inhibiting deep side-reactions. Besides, after phosphine treatment of catalysts, the vanadium species tend to exist in lower valences, which are more reactive in dehydrogenation and can retain a stable reactivity. However, higher phosphorus content could also lead to weaker vanadium-support interactions and causes drastic decline in initial activity of catalysts, so a balance between initial reactivity and stability has to be achieved at a proper low phosphorous doping amount.

4. Conclusions

Vanadium based alumina catalyst was prepared by incipient wetness impregnation and modified with phosphine at 573K. The parent catalyst showed good initial reactivity but deactivated quickly due to coke formation on active sites. As the content of phosphorus increased, the initial reactivity

decreased but the stability of catalyst was improved. Sample with the highest phosphorus content showed negligible deactivation during 8 h of reaction.

The superior role of phosphorus in maintaining propane dehydrogenation reactivity was analyzed. Synergy of surface acidic properties, electronic and geometric effects after phosphine modification accounted for the stability enhancement. Compared to conventional phosphate impregnation, phosphine interacted extensively with alumina support and vanadium species without causing structural destructions. The insertion of phosphorus into polymerized vanadium species decreased polymerization degree and formed more isolated vanadium species, which has lower dehydrogenation reactivity. Furthermore, it weakened the interaction between vanadium species and alumina, and also reduced initial reactivity of the catalysts. However, weakened vanadium-support interaction made vanadium sites more repulsive to active intermediates and propylene products, which can desorb more easily from the catalysts surface. More isolated vanadium species also expanded the distance between active propylene intermediates and reduced the possibility of oligomerization, thus inhibited coking of the catalysts. Besides, phosphorus modification maintained more strong Lewis acid sites of alumina support and stabilized lower valence vanadium, which is also beneficial for retaining a stable reactivity during PDH reactions.

In summary, doping of phosphorus in catalyst leads to decrease of initial reactivity but enhanced stability of VO_x/Al_2O_3 in PDH reactions. To obtain a balance between initial reactivity and catalytic stability, phosphorus with low amount has to be used so as to gain better propylene yield within a relatively long period.

Acknowledgements

This work was financially supported by the National Key Research and Development Program of China (2017YFB0306600), the Joint Funds of the National Natural Science Foundation of China and China National Petroleum Corporation (U1362202), Natural Science Foundation of China (51601223, 21206195, U1510109), the Fundamental Research Funds for the Central Universities (17CX05018, 17CX02056, 14CX02050A, 14CX02123A), Shandong Provincial Natural Science Foundation (ZR2017MB003) and State Key Laboratory of Heavy Oil Processing Fund (SKLZZ-2017008).

Appendix A. Supplementary data

By-products analysis, TG-DTA, EDX-mapping, Acid properties, XRD, N_2 adsorption.

References

[1] J.J. Sattler, J. Ruiz-Martinez, E. Santillan-Jimenez, B.M. Weckhuysen, Catalytic dehydrogenation of light alkanes on metals and metal oxides, Chem. Rev., 114 (2014) 10613-10653.
[2] S. Yusuf, L. Neal, V. Haribal, M. Baldwin, H.H. Lamb, F. Li, Manganese silicate based redox catalysts for greener ethylene production via chemical looping-oxidative dehydrogenation of ethane, Appl. Catal. B: Environ., 232 (2018) 77-85.
[3] S. Han, T. Otroshchenko, D. Zhao, H. Lund, N. Rockstroh, T.H. Vuong, J. Rabeah, U. Rodemerck, D. Linke, M. Gao, G. Jiang, E.V. Kondratenko, The effect of ZrO_2 crystallinity in $CrZrO_x/SiO_2$ on non-oxidative propane dehydrogenation, Appl. Catal. A: Gen., 590 (2020) 117350.
[4] O.O. James, S. Mandal, N. Alele, B. Chowdhury, S. Maity, Lower alkanes dehydrogenation: Strategies and reaction routes to corresponding alkenes, Fuel Process. Technol., 149 (2016) 239-255.
[5] L. Cao, P. Dai, L. Zhu, L. Yan, R. Chen, D. Liu, X. Gu, L. Li, Q. Xue, X. Zhao, Graphitic carbon nitride catalyzes selective oxidative dehydrogenation of propane, Appl. Catal. B: Environ., 262 (2020) 118277.
[6] Y. Liu, L. Luo, Y. Gao, W. Huang, CeO_2 morphology-dependent NbO_x-CeO_2 interaction, structure and catalytic performance of NbO_x/CeO_2 catalysts in oxidative dehydrogenation of propane, Appl. Catal. B: Environ., 197 (2016) 214-221.
[7] M.A. Atanga, F. Rezaei, A. Jawad, M. Fitch, A.A. Rownaghi, Oxidative dehydrogenation of propane to propylene with carbon dioxide, Appl. Catal. B: Environ., 220 (2018) 429-445.

[8] C. Xiong, S. Chen, P. Yang, S. Zha, Z.-J. Zhao, J. Gong, Structure-Performance Relationships for Propane Dehydrogenation over Aluminum Supported Vanadium Oxide, ACS Catal., 9 (2019) 5816-5827.
[9] K. Searles, G. Siddiqi, O.V. Safonova, C. Coperet, Silica-supported isolated gallium sites as highly active, selective and stable propane dehydrogenation catalysts, Chem. Sci., 8 (2017) 2661-2666.
[10] Y. Dai, J. Gu, S. Tian, Y. Wu, J. Chen, F. Li, Y. Du, L. Peng, W. Ding, Y. Yang, γ-Al_2O_3 sheet-stabilized isolate Co^{2+} for catalytic propane dehydrogenation, J. Catal., 381 (2020) 482-492.
[11] K. Searles, K.W. Chan, J.A. Mendes Burak, D. Zemlyanov, O. Safonova, C. Copéret, Highly Productive Propane Dehydrogenation Catalyst Using Silica-Supported Ga–Pt Nanoparticles Generated from Single-Sites, J. Am. Chem. Soc., 140 (2018) 11674-11679.
[12] C.A. Carrero, R. Schloegl, I.E. Wachs, R. Schomaecker, Critical Literature Review of the Kinetics for the Oxidative Dehydrogenation of Propane over Well-Defined Supported Vanadium Oxide Catalysts, ACS Catal., 4 (2014) 3357-3380.
[13] U. Rodemerck, M. Stoyanova, E.V. Kondratenko, D. Linke, Influence of the kind of VO_x structures in VO_x/MCM-41 on activity, selectivity and stability in dehydrogenation of propane and isobutane, J. Catal., 352 (2017) 256-263.
[14] P. Hu, W.-Z. Lang, X. Yan, X.-F. Chen, Y.-J. Guo, Vanadium-doped porous silica materials with high catalytic activity and stability for propane dehydrogenation reaction, Appl. Catal. A: Gen., 553 (2018) 65-73.
[15] Y. Sun, Y. Wu, H. Shan, G. Wang, C. Li, Studies on the promoting effect of sulfate species in catalytic dehydrogenation of propane over Fe_2O_3/Al_2O_3 catalysts, Catal. Sci. Technol., 5 (2015) 1290-1298.
[16] G. Wang, N. Sun, C. Gao, X. Zhu, Y. Sun, C. Li, H. Shan, Promoting mechanism of sulfur addition in catalytic dehydrogenation of isobutane over Mo/$MgAl_2O_4$ catalysts, Appl. Catal. A: Gen., 478 (2014) 71-80.
[17] S. Tan, B. Hu, W.-G. Kim, S.H. Pang, J.S. Moore, Y. Liu, R.S. Dixit, J.G. Pendergast, D.S. Sholl, S. Nair, C.W. Jones, Propane Dehydrogenation over Alumina-Supported Iron/Phosphorus Catalysts: Structural Evolution of Iron Species Leading to High Activity and Propylene Selectivity, ACS Catal., 6 (2016) 5673-5683.
[18] M. Sun, D. Nicosia, R. Prins, The effects of fluorine, phosphate and chelating agents on hydrotreating catalysts and catalysis, Catal. Today, 86 (2003) 173-189.
[19] S.-F. Pan, J.-L. Yin, X.-L. Zhu, X.-J. Guo, P. Hu, X. Yan, W.-Z. Lang, Y.-J. Guo, P-modified microporous carbon nanospheres for direct propane dehydrogenation reactions, Carbon, 152 (2019) 855-864.
[20] J. Horáček, U. Akhmetzyanova, L. Skuhrovcová, Z. Tišler, H. de Paz Carmona, Alumina-supported MoN_x, MoC_x and MoP_x catalysts for the hydrotreatment of rapeseed oil, Appl. Catal. B: Environ., 263 (2020) 118328.
[21] D. Liu, A. Wang, C. Liu, R. Prins, Bulk and Al_2O_3-supported Ni_2P HDS catalysts prepared by separating the nickel and hypophosphite sources, Catal. Commun., 77 (2016) 13-17.
[22] G. Liu, Z.-J. Zhao, T. Wu, L. Zeng, J. Gong, Nature of the Active Sites of VO_x/Al_2O_3 Catalysts for Propane Dehydrogenation, ACS Catal., 6 (2016) 5207-5214.
[23] G.A.H. Mekhemer, A.K.H. Nohman, N.E. Fouad, H.A. Khalaf, Surface to bulk characterization of phosphate modified aluminas, Colloids Surf. A Physicochem. Eng. Asp., 161 (2000) 439-446.

[24] C. Morterra, G. Magnacca, P.P. Demaestri, Surface Characterization of Modified Aluminas: III. Surface-Features of PO^{4-} Doped Al_2O_3, J. Catal., 152 (1995) 384-395.
[25] X. Liu, R.E. Truitt, DRFT-IR Studies of the Surface of γ-Alumina, J. Am. Chem. Soc., 119 (1997) 9856-9860.
[26] D.T. Lundie, A.R. McInroy, R. Marshall, J.M. Winfield, P. Jones, C.C. Dudman, S.F. Parker, C. Mitchell, D. Lennon, Improved Description of the Surface Acidity of η-Alumina, J. Phys. Chem. B, 109 (2005) 11592-11601.
[27] J. Dong, J. Wang, J. Wang, M. Yang, W. Li, M. Shen, Enhanced thermal stability of palladium oxidation catalysts using phosphate-modified alumina supports, Catal. Sci. Technol., 7 (2017) 5038-5048.
[28] B. Grzybowska-Świerkosz, Active centres on vanadia-based catalysts for selective oxidation of hydrocarbons, Appl. Catal. A: Gen., 157 (1997) 409-420.
[29] S.-W. Choi, W.-G. Kim, J.-S. So, J.S. Moore, Y. Liu, R.S. Dixit, J.G. Pendergast, C. Sievers, D.S. Sholl, S. Nair, C.W. Jones, Propane dehydrogenation catalyzed by gallosilicate MFI zeolites with perturbed acidity, J. Catal., 345 (2017) 113-123.
[30] U. Rodemerck, E.V. Kondratenko, T. Otroshchenko, D. Linke, Unexpectedly high activity of bare alumina for non-oxidative isobutane dehydrogenation, Chem. Commun., 52 (2016) 12222-12225.
[31] U. Rodemerck, S. Sokolov, M. Stoyanova, U. Bentrup, D. Linke, E.V. Kondratenko, Influence of support and kind of VO_x species on isobutene selectivity and coke deposition in non-oxidative dehydrogenation of isobutane, J. Catal., 338 (2016) 174-183.
[32] C. Gannoun, A. Turki, H. Kochkar, R. Delaigle, P. Eloy, A. Ghorbel, E.M. Gaigneaux, Elaboration and characterization of sulfated and unsulfated V_2O_5/TiO_2 nanotubes catalysts for chlorobenzene total oxidation, Appl. Catal. B: Environ., 147 (2014) 58-64.
[33] Y. Mizukoshi, T. Okajima, N. Masahashi, Local structure of vanadium in Ti-6Al-4V alloy anodized in acetic acid aqueous solution and its contribution to visible light response in photocatalysis, Appl. Catal. B: Environ., 162 (2015) 180-186.
[34] P. Bai, Z. Ma, T. Li, Y. Tian, Z. Zhang, Z. Zhong, W. Xing, P. Wu, X. Liu, Z. Yan, Relationship between Surface Chemistry and Catalytic Performance of Mesoporous gamma-Al_2O_3 Supported VO_x Catalyst in Catalytic Dehydrogenation of Propane, ACS Appl. Mater. Interfaces, 8 (2016) 25979-25990.
[35] P. Hu, W.-Z. Lang, X. Yan, L.-F. Chu, Y.-J. Guo, Influence of gelation and calcination temperature on the structure-performance of porous VO_x-SiO_2 solids in non-oxidative propane dehydrogenation, J. Catal., 358 (2018) 108-117.
[36] X. Wu, X. Yu, Z. Huang, H. Shen, G. Jing, MnO_x-decorated VO_x/CeO_2 catalysts with preferentially exposed {110} facets for selective catalytic reduction of NO_x by NH_3, Appl. Catal. B: Environ., 268 (2020) 118419.
[37] K. Fukudome, T. Suzuki, Highly Selective Oxidative Dehydrogenation of Propane to Propylene over VO_x-SiO_2 Catalysts, Catal. Surv. from Asia, 19 (2015) 172-187.
[38] Z. Wu, H.-S. Kim, P.C. Stair, S. Rugmini, S.D. Jackson, On the Structure of Vanadium Oxide Supported on Aluminas: UV and Visible Raman Spectroscopy, UV-Visible Diffuse Reflectance Spectroscopy, and Temperature-Programmed Reduction Studies, J. Phys. Chem. B, 109 (2005) 2793-2800.
[39] N. Jeon, H. Choe, B. Jeong, Y. Yun, Propane dehydrogenation over vanadium-doped zirconium oxide catalysts, Catal. Today, (2019).

[40] H. Zhao, C. Zuo, D. Yang, C. Li, S. Zhang, Effects of Support for Vanadium Phosphorus Oxide Catalysts on Vapor-Phase Aldol Condensation of Methyl Acetate with Formaldehyde, Ind. Eng. Chem. Res., 55 (2016) 12693-12702.
[41] N.P. Rajan, G.S. Rao, B. Putrakumar, K.V.R. Chary, Vapour phase dehydration of glycerol to acrolein over vanadium phosphorous oxide (VPO) catalyst, RSC Adv., 4 (2014) 53419-53428.
[42] H.-Y. Wu, P. Jin, Y.-f. Sun, M.-H. Yang, C.-J. Huang, W.-Z. Weng, H.-L. Wan, Enhancing catalytic performance of phosphorus-modified ceria supported VPO catalysts for n-butane oxidation, J. Mol. Catal. A: Chem., 414 (2016) 1-8.
[43] B.M. Weckhuysen, D.E. Keller, Chemistry, spectroscopy and the role of supported vanadium oxides in heterogeneous catalysis, Catal. Today, 78 (2003) 25-46.
[44] J. Jian, K. You, Q. Luo, H. Gao, F. Zhao, P. Liu, Q. Ai, H.a. Luo, Supported Ni-Al-VPO/MCM-41 As Efficient and Stable Catalysts for Highly Selective Preparation of Adipic Acid from Cyclohexane with NO_2, Ind. Eng. Chem. Res., 55 (2016) 3729-3735.
[45] A. Martin, C. Janke, V.N. Kalevaru, Ammoxidation of 3-picoline to nicotinonitrile over VPO catalysts, Appl. Catal. A: Gen., 376 (2010) 13-18.
[46] F. Cavani, S. Ligi, T. Monti, F. Pierelli, F. Trifirò, S. Albonetti, G. Mazzoni, Relationship between structural/surface characteristics and reactivity in n-butane oxidation to maleic anhydride, Catal. Today, 61 (2000) 203-210.
[47] L. Kőrösi, I. Dékány, Preparation and investigation of structural and photocatalytic properties of phosphate modified titanium dioxide, Colloids Surf. A Physicochem. Eng. Asp., 280 (2006) 146-154.
[48] S. Li, W. Huang, H. Xu, T. Chen, Y. Ke, Z. Qu, N. Yan, Alkali-induced deactivation mechanism of V_2O_5-WO_3/TiO_2 catalyst during selective catalytic reduction of NO by NH_3 in aluminum hydrate calcining flue gas, Appl. Catal. B: Environ., 270 (2020) 118872.
[49] Y.P. Tian, P. Bai, S.M. Liu, X.M. Liu, Z.F. Yan, VO_x-K_2O/γ-Al_2O_3 catalyst for nonoxidative dehydrogenation of isobutane, Fuel Process. Technol., 151 (2016) 31-39.
[50] J. Haber, Fifty years of my romance with vanadium oxide catalysts, Catal. Today, 142 (2009) 100-113.
[51] Y. Wu, X. Liu, D. Han, X. Song, L. Shi, Y. Song, S. Niu, Y. Xie, J. Cai, S. Wu, J. Kang, J. Zhou, Z. Chen, X. Zheng, X. Xiao, G. Wang, Electron density modulation of $NiCo_2S_4$ nanowires by nitrogen incorporation for highly efficient hydrogen evolution catalysis, Nat. Commun., 9 (2018) 1425.
[52] M. Aly, E.L. Fornero, A.R. Leon-Garzon, V.V. Galvita, M. Saeys, Effect of Boron Promotion on Coke Formation during Propane Dehydrogenation over Pt/γ-Al_2O_3 Catalysts, ACS Catal., (2020) 5208-5216.
[53] J. Gong, Z. Zhao, T. Wu, C. Xiong, G. Sun, R. Mu, Z. Liang, Hydroxyl-mediated Non-oxidative Propane Dehydrogenation over VO_x/Al_2O_3 Catalysts with Promoted Stability, Angew. Chem. Int. Ed., 57 (2018).

Figures

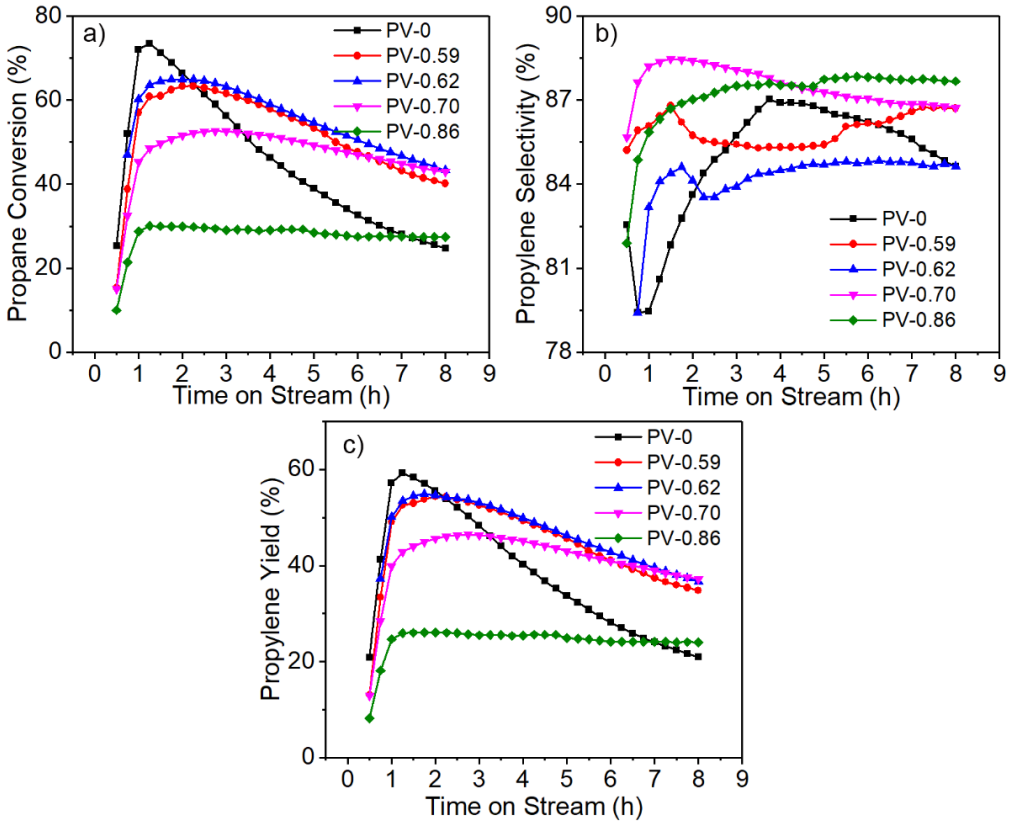

Fig. 1. Catalytic performance of parent and phosphine modified catalysts in propane dehydrogenation reactions (a) propane conversion, (b) propylene selectivity, and (c) propylene yield as a function of time on stream.

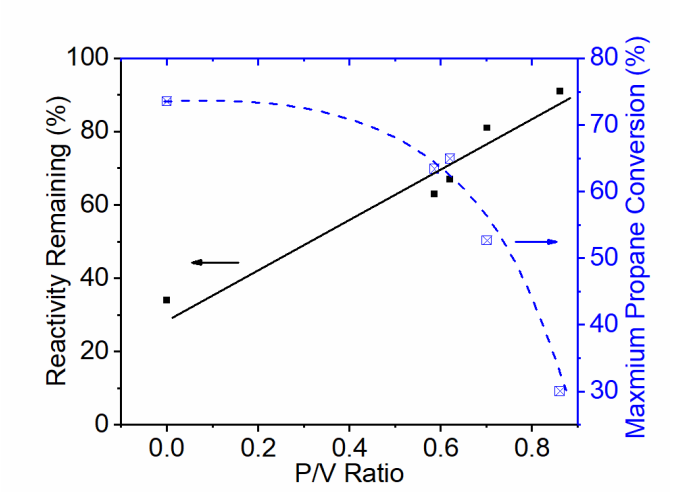

Fig. 2. Reactivity remaining and the maximum propane conversions of parent and phosphine modified catalysts.

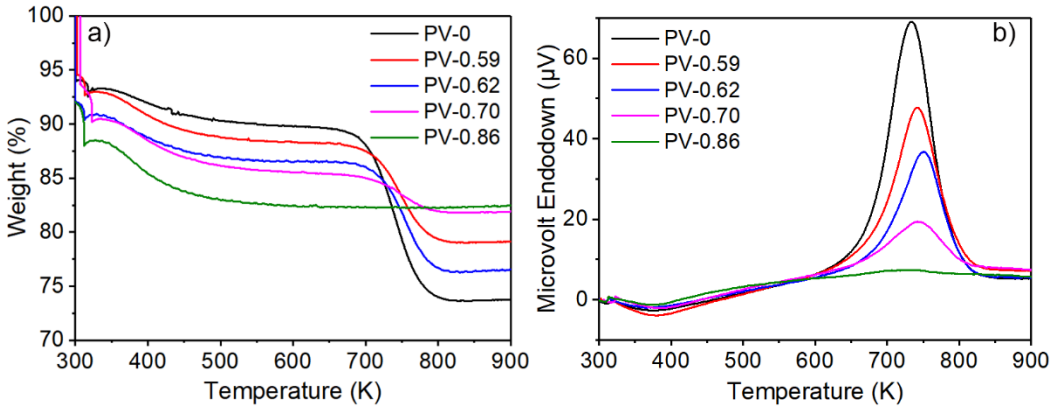

Fig. 3. TG-DTA profiles of used parent and phosphine modified catalysts: (a) weight loss and (b) microvolt endodown as a function of temperature.

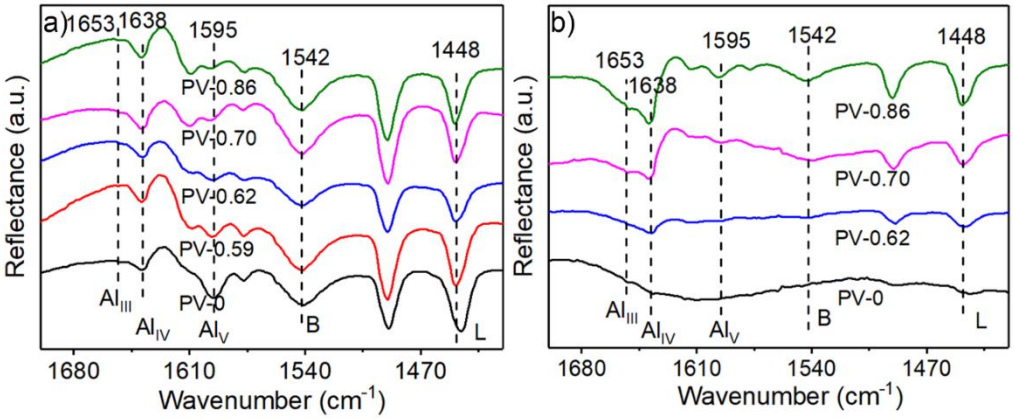

Fig. 4. Py-DRIFTS spectra of (a) fresh and (b) used parent and phosphine modified catalysts.

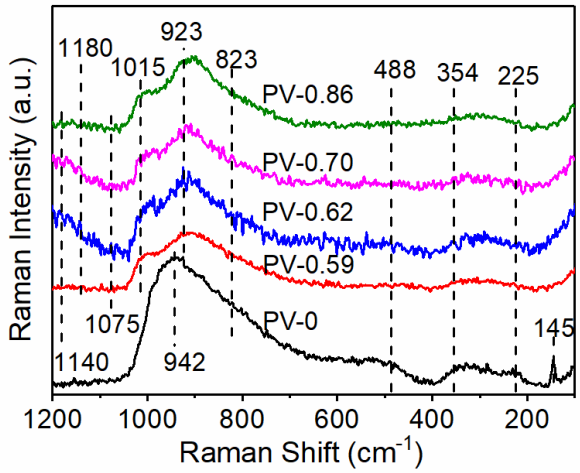

Fig. 5. Raman spectra of parent and phosphine modified catalysts.

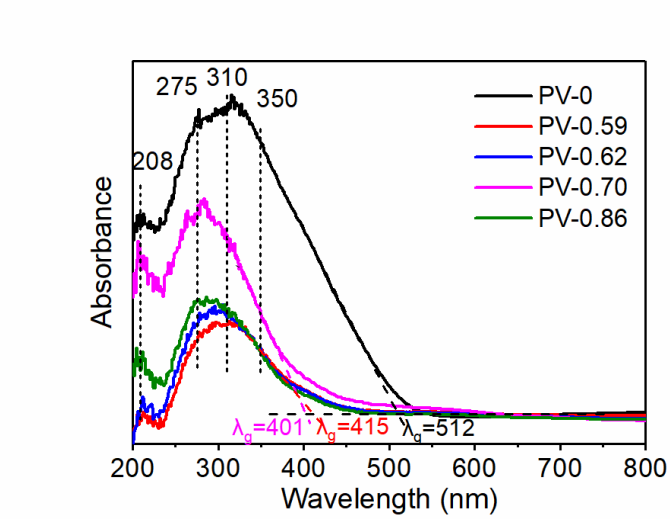

Fig. 6. UV-Vis spectra of parent and phosphine modified catalysts.

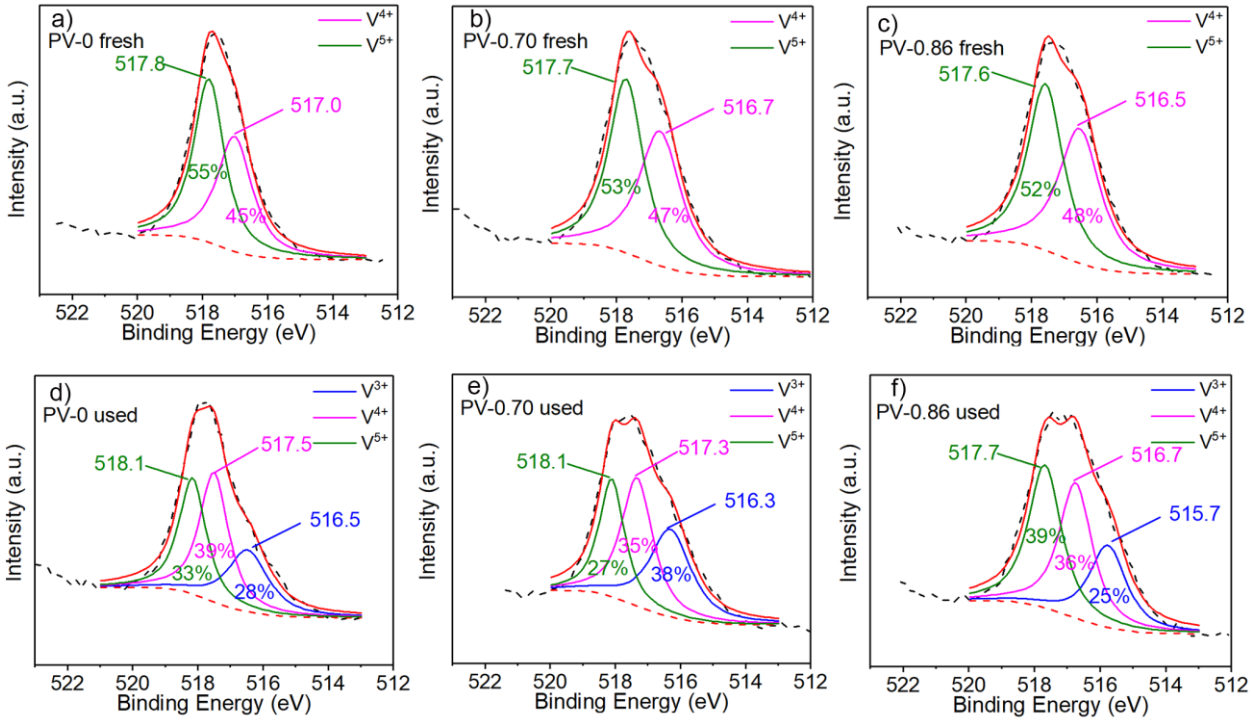

Fig. 7. V 2p3/2 XPS spectra of fresh and used parent and phosphine modified catalysts: (a) PV-0 fresh, (b) PV-0.70 fresh, (c) PV-0.86 fresh, (d) PV-0 used, (e) PV-0.70 used, (f) PV-0.86 used.